Phenolic ester-decorated cellulose nanocrystals as UV-absorbing nano-reinforcement in polyvinyl alcohol films

David Joram Mendoza[a], Christine Browne[a], Vikram Singh Raghuwanshi[a], Louis M. M. Mouterde[b], George P. Simon[c,*], Florent Allais[a,b,*] and Gil Garnier[a,b,*]

[a]15 Alliance Lane (Building 59), Bioresource Processing Research Institute of Australia (BioPRIA), Department of Chemical Engineering, Monash University, Clayton, VIC 3800, Australia

[b]URD Agro-Biotechnologies Industrielles (ABI), CEBB, AgroParisTech, 51110, Pomacle, France

[c]14 Alliance Lane (Building 72), Department of Materials Science and Engineering, Monash University, Clayton, VIC 3800, Australia

*Corresponding authors:

Gil Garnier, email address: gil.garnier@monash.edu, Tel.: +61 3 9905 3456

George P. Simon, email address: george.simon@monash.edu, Tel.: +61 3 9905 4934

Florent Allais, email address: florent.allais@agroparistech.fr, Tel.: +33 (0)6 33698126

Keywords: cellulose nanocrystals, phenolic esters, *p*-hydroxycinnamate esters, click-chemistry, nanocomposites, polyvinyl alcohol

ABSTRACT

Grafting novel and nature-inspired phenolic esters onto cellulose nanocrystals (CNCs) provides nanofibers with excellent protection against UV radiation when incorporated into a polymer matrix. In this work, cellulose nanocrystals decorated with a novel UV-absorbing phenolic diester (CNC-diethyl ferulate or CNC-DEF) obtained *via* a click-type copper-catalyzed azide/alkyne cycloaddition (CuAAC) reaction were incorporated into a polyvinyl alcohol (PVA) matrix to produce transparent films with excellent photostability and UV-absorbing properties. PVA films filled with 20 wt% CNC-DEF exhibited complete UV protection (0% transmittance) and high transparency in the visible region (70-90% transmittance). In contrast, PVA films loaded with the pristine CNCs do not show any UV shielding properties. Importantly, the grafting of DEF moieties on CNCs significantly aids the dispersion of the phenolic diester in the aqueous PVA matrix, which was not achieved with DEF blended with PVA. Mechanical tests also show the addition of 20 wt% CNC-DEF in PVA to increase the tensile strength and modulus by 91% and 150%, respectively, relative to neat PVA. The oxygen barrier properties of the composite film also improve with CNC-DEF addition. This study shows the great potential of the phenolic-ester decorated CNCs as dispersible, multifunctional UV-absorbing nano-reinforcement in PVA films for industrial and packaging applications.

Supporting Information. Synthesis of diethyl ferulate, alkyne-modified diethyl ferulate and azide-modifed CNCs; ^{1}H and ^{13}C NMR spectra of diethyl ferulate and alkyne-modified diethyl ferulate; photographs of suspensions of CNC, CNC-DEF, and DEF in PVA solution; Optical profilometry analysis of PVA, PVA+CNC, and PVA-CNC-DEF films.

INTRODUCTION

In nature, plants and many biological systems manufacture tough and high-performance structural biocomposites composed of a matrix reinforced with fibrous biopolymers. This has inspired many researchers to combine (bio)polymers with a broad range of other components to develop multifunctional polymer nanocomposites. The addition of functional nanofibers can significantly improve the properties of a polymeric composite material as they confer new features including excellent mechanical strength and toughness, high thermal stability, low water/gas permeability, while retaining good optical properties[1-4].

A widely-used polymer is polyvinyl alcohol (PVA) - a hydrophilic and semi-crystalline polymer - derived from the hydrolysis of polyvinyl esters. In addition to its use as material in a broad range of industries, PVA has been extensively explored as matrix for nanocomposites due to its water-solubility, excellent film-forming property, abundance and low cost [5]. Many organic and inorganic additives were blended with PVA, such as metal oxide nanoparticles [6, 7], graphene oxide [8], halloysite [9], starch [7], cellulose[10, 11] and carbon nanotubes. These nanofillers can provide additional functionalities to PVA such as optical, mechanical and electrical properties. Due to its good water solubility, PVA is an excellent polymeric matrix to incorporate hydrophilic functional nanofillers.

Recently, PVA was combined with nanocellulose, a class of nanostructured cellulosic materials that refers to cellulose nanocrystals (CNCs), cellulose nanofibers (CNFs), and bacterial nanocellulose (BNC) [12, 13]. Nanocellulose has been widely investigated as a nanofiber because of its excellent mechanical properties, unique optical properties, tunable surface chemistry, and biodegradability [14, 15]. PVA is chemically-compatible with cellulose due to its hydrophilicity and free hydroxyl moieties which facilitate interfacial interactions through hydrogen bonding. For example, Fortunati et al.[16] prepared PVA-CNC composite films and reported an important improvement in the tensile strength relative to neat PVA. In addition, Xu et al.[17] described that the reinforcement of CNCs and hemicellulose in PVA films significantly reduced its water-vapor permeability. Liu et al.[18] also blended cellulose nanofibrils with PVA to prepare transparent composite films and reported an increase in the crystallinity, mechanical strength, and thermal stability of the PVA films.

Recently, we reported a new and innovative synthetic route to decorate cellulose nanocrystals with a family of UV-absorbing phenolic esters using a click-type reaction[19]. CNCs were grafted with nature-inspired, plant-derived *p*-hydroxycinnamate esters and *p*-hydroxycinnamate diesters which exhibit excellent UV absorption and photostability. In addition, these phenolic compounds showed potential as strong antioxidant, antimicrobial, and other bioactive properties[20-22]. Similar to pristine CNCs, we envisage that the phenolic ester-

grafted CNCs can act as an excellent reinforcing and UV-absorbing functional nanofiber in PVA films. Polymer films with UV-absorption properties have become increasingly important due to the detrimental effects of UV irradiation on human health and most biological systems. Indeed, PVA was functionalized with different UV-absorbing additives to develop anti-UV materials. For example, metallic inorganic nanoparticles such as ZnO and TiO_2 were previously blended with PVA [23, 24]. While they offer advantages such as efficient UV absorption and long-life cycle, these nanoparticles pose some health and environmental concerns[25]. For example, previous reports have shown that these nanoparticles can induce the photodegradation of polymeric matrices[26]. On the contrary, PVA films loaded with bio-based additives, such as cinnamate derivatives[27, 28] and lignin[23, 29, 30], offer comparable UV protection without any expected detrimental effects on the polymer matrix and the environment. For instance, significant UV absorption was observed after the addition of different concentrations of cinnamate-based CNCs [28, 31] in PVA films. However, the effect of these CNC derivatives on the oxygen barrier properties of the PVA composite films were not studied.

Here, we report the application of novel phenolic ester-decorated CNCs as multifunctional nanofillers in polyvinyl alcohol films. In particular, we have synthesized diethyl 2-(4-hydroxy-3-methoxybenzylidene)malonate or diethyl ferulate (DEF) from benzaldehyde using a green Knoevenagel condensation reaction. Diethyl ferulate was grafted onto CNCs *via* a copper-catalyzed azide/alkyne cycloaddition (CuAAC) reaction and the decorated CNCs reinforced in PVA films using a simple solution casting method. We highlight in this study the role of CNCs in aiding the dispersion of the water-insoluble phenolic compound in the PVA matrix. Composite films with pristine CNCs and grafted CNCs are extensively characterized to quantify the effects of grafting on the properties of the films. We also show the improvements in the PVA films after grafted CNC reinforcement in terms of UV-blocking property, photostability, mechanical performance, and oxygen permeability. Our objective is to develop performant and nature-inspired functional nanofibrillar additives in polymeric films scalable for industrial and packaging applications.

EXPERIMENTAL

Materials

All chemicals are analytical grade and used without further purification. Polyvinyl alcohol (Mowiol® 4-98, $M_w \approx 27{,}000$ g/mol), ferulic acid, copper (II) bromide ($CuBr_2$), potassium carbonate (K_2CO_3), *p*-toluenesulfonyl chloride, proline, ascorbic acid, and sodium azide (NaN_3) were purchased from Sigma-Aldrich. Absolute ethanol, *N*,*N*-dimethylformamide (DMF) and triethylamine were acquired from Merck. Propargyl bromide (80 wt% in toluene) were purchased from Acros Organics. Diethyl malonate and pyridine were acquired from Tokyo

Chemical Industries (TCI). Sulfuric acid-hydrolysed cellulose nanocrystals (98% dry powder, 0.8-0.9% sulfur) were purchased from the University of Maine, USA. Diethyl ferulate (DEF) was synthesized *via* proline-mediated Knoevenagel condensation of vanillin and diethyl malonate (Figure S1) as reported previously[32].

Synthesis of alkyne-modified diethyl ferulate

Diethyl ferulate was modified with a terminal alkyne moiety *via* Williamson etherification with propargyl bromide (Figure S2) as reported previously[19, 33]. Briefly, diethyl ferulate (1 eq) was dissolved in 10 mL anhydrous DMF in an ice bath. K_2CO_3 (1 eq) and propargyl bromide (1.2 eq) were then added and the reaction mixture was stirred overnight at room temperature under nitrogen. The reaction was monitored by thin-layer chromatography (TLC) using pre-coated aluminum sheets (Silica gel 60 F254, Merck Germany) and spots were visualized under UV light. Purification was performed by flash chromatography (Puriflash 4100, Interchim with pre-packed silica gel column) with cyclohexane/ethyl acetate (8:2) as eluent. ^{1}H and ^{13}C NMR NMR spectra of the DEF-alkyne derivative in $(CD_3)_2CO$ were recorded using Fourier 300 Bruker at 300 MHz (residual signal at δ = 2.05 ppm) and 75 MHz (residual signal at δ = 206.26 and 29.84 ppm) at 20 °C, respectively. The spectra and assignments of the DEF-alkyne derivative (85% yield) are shown in Figure S3-S4.

Synthesis of DEF-grafted CNCs (CNC-DEF)

Cellulose nanocrystals (CNCs) were grafted with DEF *via* copper(I)-catalyzed azide-alkyne cycloaddition reaction as reported previously[19]. The CNCs were modified with azide groups following two major steps (Figure S5): a) tosylation with *p*-toluenesulfonyl chloride at room temperature for 48 h and b) azidation with NaN_3 at 100 ˚C for 24 h. Surface-azidized CNCs (CNC-N_3) were obtained in a 96% yield. Alkyne-modified DEF (0.4 g, 1 eq) and CNC-N_3 (0.4 g, 1 eq) were suspended in DMF. A DMF solution containing $CuBr_2$ (56 mg), ascorbic acid (160 mg), and triethylamine (400 µL) was then slowly added and the reaction mixture was stirred at 60 ˚C for 24 h. The CNCs were precipitated with 200 mL of ethanol and were repeatedly centrifuged (11,000 rpm, 20 mins) and washed with ethanol and water. The CNCs were dialysed against Milli-Q water for 5 days and freeze-dried for 2 days. Approximately 0.4 g of the click product was obtained (50% yield). CNC-DEF suspensions (2 wt%) were prepared by suspending a known amount of the powder in water followed by ultrasonication for 5 minutes at 19.5 kHz and 70% amplitude (ON/OFF, 5 s).

Preparation of PVA films

PVA (0.2 g) was initially dissolved in water by heating at 90 ˚C for 1 hr. The PVA solution was allowed to slowly cool down to room temperature and the corresponding amount of CNC-DEF aqueous suspension (2 wt%) added. The mixture was stirred at room temperature for 16h,

ultrasonicated for 5 minutes, and casted on polystyrene petri dish (40 mm diameter). The samples were then dried at 23 ˚C and 50% humidity for 5 days. The concentrations of CNC-DEF in the PVA films were controlled at 0-20 wt%. For comparison, PVA films loaded with the same concentrations of pristine CNCs were also prepared.

Characterization

FTIR

FTIR spectra of the PVA films were generated using an Agilent Technologies Cary 630 FTIR equipped with a diamond ATR accessory. The spectra were recorded at a resolution of 4 cm^{-1} with 32 scans in the range of 4000-500 cm^{-1}.

Elemental Analysis and Degree of Substitution

The degree of substitution (DS) of the CNC derivatives was quantified through elemental analysis (Thermo Scientific FlashSmart CHNS). The DS of CNC-N_3 was directly calculated from the %N whilst the DS of CNC-DEF was quantified based on %C and calculated using equation (1) as previously reported[34]:

$$DS = \frac{6 \times M_C - \%C \times M_{AGU}}{M_g \times \%C - M_{Cg}} \qquad (1)$$

where 6 x Mc is the carbon mass of one anhydroglucose unit (72.07 g/mol), M_{AGU} is the mass of anhydroglucose unit (162.14 g/mol), M_g is the mass of the grafted molecule (344.35 g/mol) and M_{Cg} is the carbon mass of the grafted molecule (204.17 g/mol).

The DS values were further converted to degree of surface substitution (DS_{surf}) equivalents using equation (2):

$$DS = R_c DS_{surf} \qquad (2)$$

assuming a CNC chain ratio (R_c) of 0.29 [35].

Contact Angle

The water contact angles (WCA) of the PVA films were determined using a contact angle instrument (Dataphysics, OCA35). The static WCA was recorded by analysing images of three water droplets (3 µL).

Dynamic Light Scattering (DLS) and Zeta Potential

DLS and zeta potential analyses of 1 wt% CNC and CNC-DEF in PVA solution were performed using a Brookhaven Nanobrook Omni particle analyzer. Measurements were performed in five replicates per sample and the average and standard deviated are reported.

UV-Vis Spectroscopy and Photostability

The optical transmittance of the PVA films were generated at 300-800 nm using an UV-Vis spectrometer (Cary 60 UV-Vis Agilent Technologies). The photostability of the PVA films was also quantified by loading film strips in quartz cuvettes, followed by irradiation at 365 nm for 2 h using a 32-W UV-lamp. The optical transmittance of the films was measured at different UV irradiation time.

SAXS

Small angle X-ray Scattering (SAXS) experiments were performed at the SAXS/WAXS beamline of the Australian Synchrotron. SAXS measurements were made in the transmission mode at the incident X-ray energy of 12 keV (λ = 1.033 Å). PILATUS 1 M detector (pixel size 172 µm × 172 µm) was used to collect the scattered X-rays placed at 7 m (q range: 0.001 and 0.1 $Å^{-1}$) from the sample position. The Scatter Brain software was used to perform data reduction and radial averaging of the SAXS curves. The final SAXS curves were plotted as scattered intensity verses scattering vector q (1/A). The q values were calibrated by the scattering curve of silver behenate.

Mechanical Tests

The PVA films (~100 µm) were cut into rectangular strips (40 mm long x 20 mm wide) and allowed to equilibrate t 23 °C and 50% RH for a minimum of 24 h. Stress-strain curves were recorded using an Instron tensile tester (model 5566) with constant rate of elongation of 10 mm/min. The Young's modulus, yield strength, and elongation at break were calculated from the curves using the Bluehill® Universal software.

Oxygen Permeability

Oxygen permeability tests were performed *via* a MOCON OXTRAN 2/22 (Minneapolis) at 25 °C, 0% relative humidity, and 1 atm. PVA films were initially cut into 1x1 cm^2 strips and masked with a standard aluminium sheet. The oxygen transmission rates were calculated using the software provided in the instrument.

Optical Profilometry

PVA films (4 x 4 cm^2) were examined under an optical profilometer (Olympus LEXT OLS 5000 Laser Confocal Microscope). The 3D surface images and average aerial roughness (S_a) of the films were generated using the instrument software (Analysis application, version 1.3.1.139).

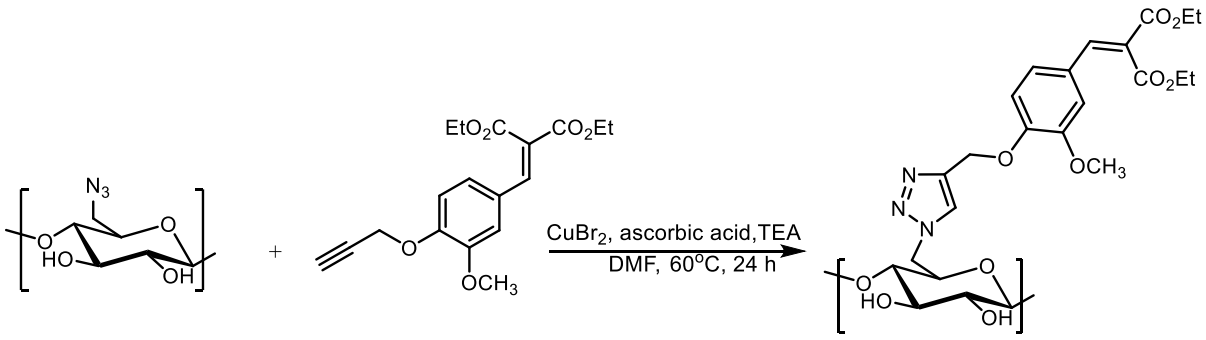
Scanning Electron Microscopy

Scanning electron microscopy (SEM) was performed using FEI Magellan 400 equipped with a field-emission source. The PVA films were mounted on carbon and coated with iridium (<1 nm) and examined at 5 kV. The cross-section was also examined by cryo-fracturing the films in liquid nitrogen.

RESULTS

Synthesis of DEF-decorated CNCs

CNCs were decorated with diethyl ferulate *via* copper(I)-catalyzed alkyne-azide cycloaddition (CuAAC) reaction as shown in Scheme 1. The reaction requires an azide group and a terminal alkyne group to form a five-membered triazole ring. Diethyl ferulate was initially modified with a terminal alkyne moiety following a simple Williamson etherification with propargyl bromide (Figure S2). CNCs, on the other hand, were functionalized with an azide group *via* 2-steps: activation of the primary hydroxyl groups by tosylation, followed by a subsequent nucleophilic substitution with the azide group. This two-step process is proven to be highly efficient as the degree of surface substitution (DS_{surf}) achieved in azide-modified CNCs (DS_{surf} =0.50) corresponds to the expected theoretical value for maximum surface substitution of primary hydroxymethyl groups on CNC surface [36-38]. The cycloaddition reaction, on the other hand, afforded DEF-grafted CNCs with a DS_{surf} of 0.31 corresponding to 62% conversion of the azide group to the triazole derivative. This result corroborates our previous study where 48-82% conversion rates were achieved[19]. The click reaction employed was demonstrated to be highly efficient, as revealed by UV-Vis, FTIR, and XPS analyses presented in our previous study [19].



Scheme 1: Copper-catalyzed click reaction of CNC-N_3 and alkyne-modified diethyl ferulate (DEF).

Incorporation of CNC-DEF in PVA matrix

Aqueous suspensions of pristine CNCs and DEF-grafted CNCs (1-20 wt%) were dispersed in PVA solutions to prepare the films. Figure S6 shows that pristine CNCs and CNC-DEF dispersed well in PVA and showed no visible aggregation which suggests the good dispersibility of both types of CNCs in the PVA matrix. Pristine CNCs and CNC-DEF dispersed in aqueous PVA solution have a hydrodynamic diameter (D_h) of 72.87± 0.57 nm and 158.51 ± 3.15 nm, respectively. Further, pristine CNCs and CNC-DEF in aqueous PVA exhibited zeta potentials of -56.23 ± 1.92 mV and -52 ± 2.19 mV, respectively. These results show that these

aqueous suspensions are highly negatively-charged and colloidally stable. For comparison, it was also attempted to suspend DEF in the PVA aqueous solution. As expected, DEF did not disperse nor dissolve in the PVA matrix primarily because of its hydrophobic nature.

The PVA solutions were casted and dried to obtain flexible, transparent, and free-standing films (Figure 1a). The films do not show any visual aggregation which suggests good dispersion of the CNCs in the PVA matrix even after prolonged drying. This is supported by optical profilometry results (Figure S7) where relatively smooth surfaces were obtained. Notably, PVA films loaded with pristine CNC remained colourless and transparent, whereas those loaded with CNC-DEF are brownish, due to the deep-yellow colour of the CNC-DEF suspension. Water contact angle measurements (Figure 1b) reveal that the addition of the CNCs and CNC-DEF in the PVA matrix is successful. PVA films loaded with pristine CNCs were slightly more hydrophilic than the neat PVA which can be attributed to the several hydroxyl groups present in cellulose. On the contrary, PVA films with CNC-DEF (20 wt%) incorporated were significantly more hydrophobic than the neat PVA and PVA+CNC films; this is as expected due to the hydrophobic character of the grafted phenolic ester.

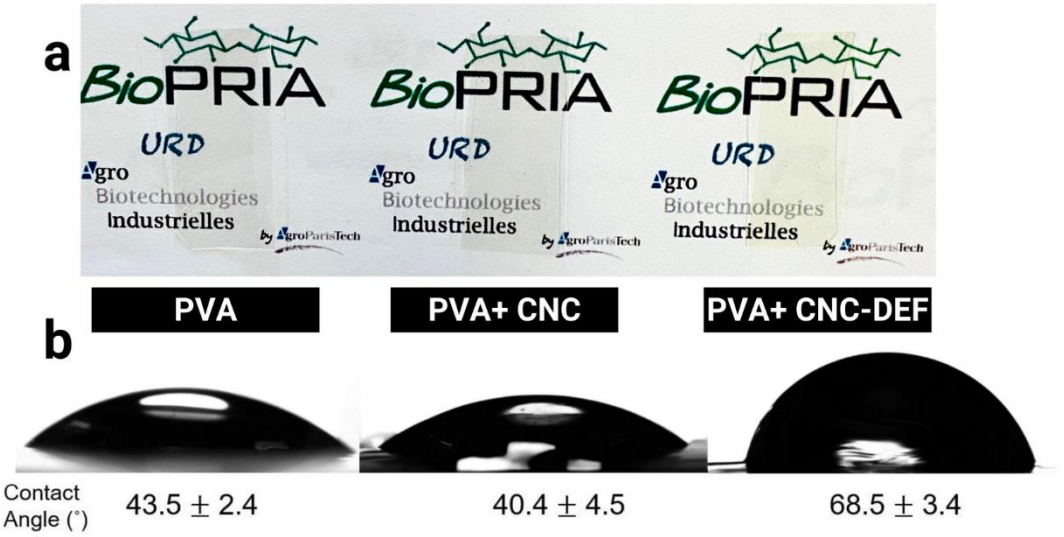


Figure 1: Photographs of **(a)** PVA, PVA +CNC (20 wt%), and PVA+CNC-DEF (20 wt%) films prepared by solution-casting. **(b)** Images of water droplets on PVA, PVA +CNC (20 wt%), and PVA+CNC-DEF (20 wt%) films and their corresponding contact angles.

Figure 2 shows the FTIR spectra of the neat PVA, PVA + CNC, and PVA + CNC-DEF films. Characteristic peaks at 3300-3200 (broad O-H stretch), 2940-2950 (C-H stretch) and 1090 (C-O stretch) cm^{-1} typical of polyvinyl alcohol[17, 39, 40] and cellulose[13, 14] were observed in all films. The peak at around 1150 cm^{-1} is attributed to the crystalline domains of PVA[39]. Films with CNC-DEF showed characteristic peaks attributed to the presence of the grafted diethyl

ferulate. A sharp peak at around 2110 cm^{-1}, arising from the unreacted azide groups in CNC, was observed[41]. The triazole ring in the grafted CNC is also evidenced by the presence of a peak at 1630 cm^{-1}. Sharp stretching bands at 1715 (α, β-unsaturated esters) and 1585 (aromatic ring) cm^{-1} also confirm the presence of DEF in the PVA matrix. These results further support that CNC-DEF is well dispersed in to the PVA matrix and no chemical reactions occurred during the preparation of the film.

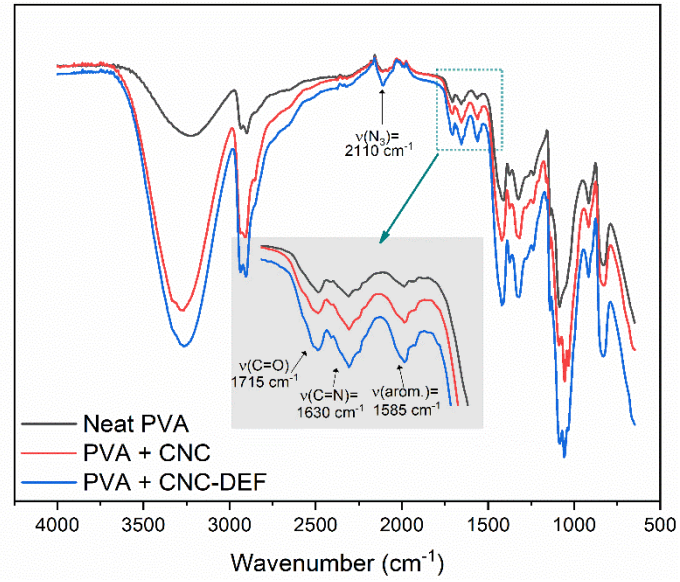


Figure 2: FTIR spectra of neat PVA, PVA + CNC (20 wt%), and PVA+CNC-DEF (20 wt%) film composites.

The effect of CNC and CNC-DEF reinforcement on the morphology of PVA films was investigated by FE-SEM analysis. As shown in Figures 3a-c, there are no significant changes in the surface of the PVA films from the addition of CNC or CNC-DEF. However, further examination of the cross-section of the films reveals significant changes in the morphology after filler reinforcement. The neat PVA displays a loose structure characterised by several voids in the range of 100-300 nm (Figure 3d). However, after the addition of CNC or CNC-DEF (Figures 3e-f), the structure became more densely compact and the voids completely disappeared. These results corroborate the findings of Xu et al. [17] where the reinforcement of hemicellulose and CNC also resulted in similar structural changes. These results illustrate that both CNC and CNC-DEF can be well dispersed into the PVA matrix.

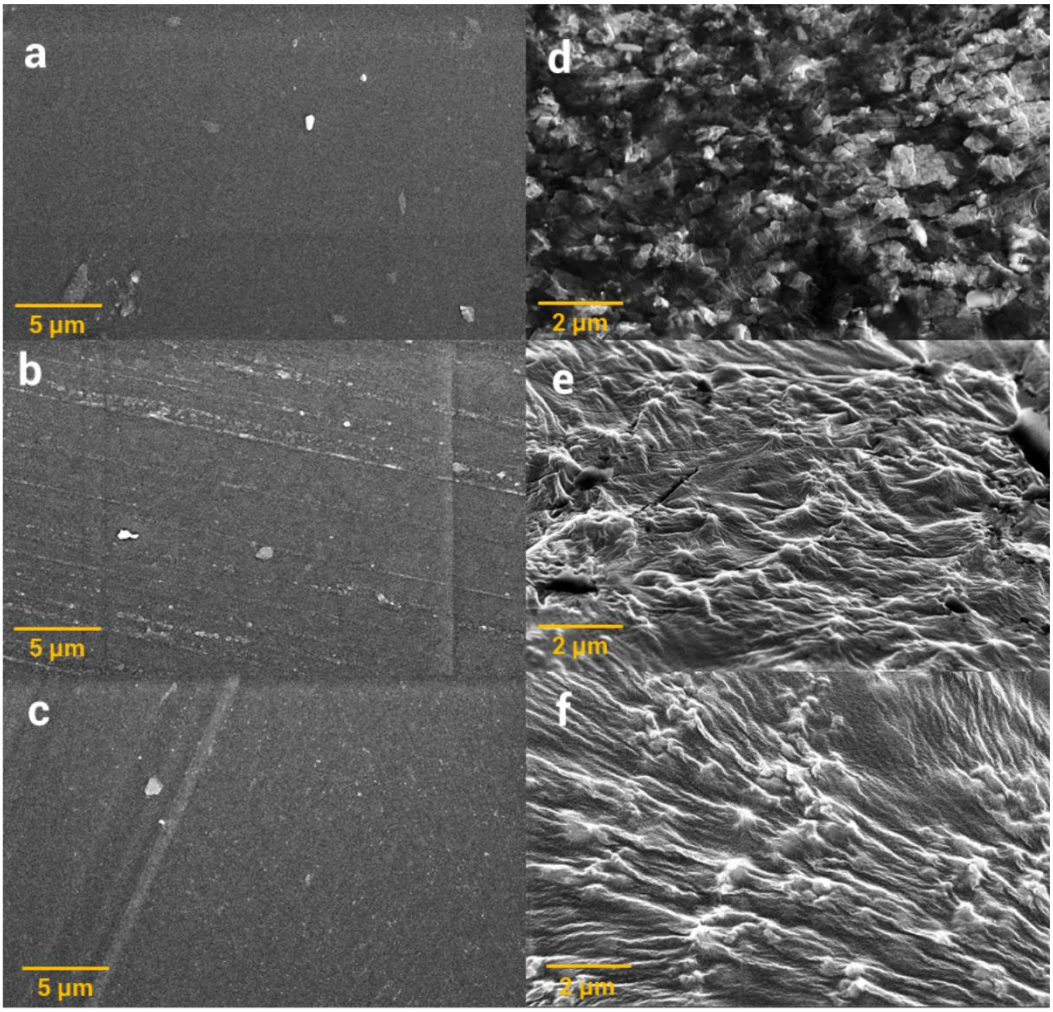


Figure 3. Morphological structure of neat PVA, PVA+CNC (20 wt%), and PVA+CNC-DEF (20 wt%) composite films. FE-SEM images of the surface of **(a)** neat PVA, **(b)** PVA+CNC, and **(c)** PVA+CNC-DEF composite films. FE-SEM images of the cross-section of cryo-fractured **(d)** neat PVA, **(e)** PVA+CNC (20 wt%), and **(f)** PVA+CNC-DEF (20 wt%) composite films.

SAXS measurements were performed to quantify any nanoscale changes in the PVA, PVC/CNC and PVC/CNC-DEF. SAXS is a powerful method to determine the structure morphology and distribution in the size range from 1-100 nm[42-44]. Figure 4 shows the SAXS curves of pure PVA film and PVA films loaded with 20% pristine CNC and 20% CNC-DEF. The neat PVA curve reveals a characteristic peak at q=0.6 nm^{-1} which corresponds to the average distance between PVA crystallites with an average length (L) of 10 nm [45]. This peak completely disappeared after the addition of pristine CNC or CNC-DEF. This suggests that the addition of CNC or CNC-DEF reduces the driving force for crystallization of PVA. This can be attributed to the formation of hydrogen bonds restraining PVA chains mobility[46].

For further analysis, the lower q values of the SAXS curves were fitted with the power law by using the equation $\ln(q) \propto q^{-\alpha}$ The value of slope (α) resembles the scattering from

the surface and internal nanostructures. The value of α between 3<α<4 reveals the surface fractals and compact structures or large aggregates with dense core and rough surface. The lower value of α between 1<α<3 describes the mass fractal structure which is the arrangement of structural elementary units in open structure. A smaller value of α means a less aggregated structure with less interparticle interaction.

For the pure PVA, the value of α is 3.8, revealing the scattering resulting from large compact structures in the PVA (Figure 4a). The other two samples of CNC and CNC-DEF incorporated into PVA show the mass fractal dimension as the value of α is between 1-2. The appearance of fractal dimensions indicating the formation of open structures. The slope of α =1.8 for PVA with the 20 wt% CNC shows the CNC rods are close to each other. However, the PVA sample with 20 wt% CNC-DEF has a reduced value of α being 1.2, indicating the CNC rods are moved away from each other and have less interactions. The SAXS intensity pattern seems like the scattering is coming from a linear (or one-dimensional) object.

The Guinier representation ($\ln(l.q)$ vs. q^2) of the SAXS data for the rod like nanostructures also confirms the CNC aggregation for the PVA+20 wt% CNC film compared to non-aggregation in the 20 wt% CNC-DEF in the PVA network (Fig 3b). The Guinier plot of the PVA-CNC sample shows the upturn/curved in the lower q value, indicating that the CNC rods are close to each other in an open polymeric structure. The radius of gyration (R_g) is evaluated from the slope of the Guinier plot and the equation $I(q) = \frac{I(0)}{q} exp\left(-\frac{q^2 {R_g}^2}{2}\right)$[47]. The increase in the scattering intensity of 20 wt% CNC indicates that the formed structure has a higher R_g of 8 nm. The sample of PVA with CNC-DEF shows a linear trend in the Guinier representation, indicating non-aggregated structures of CNC-DEF with R_g of 5.6 nm.

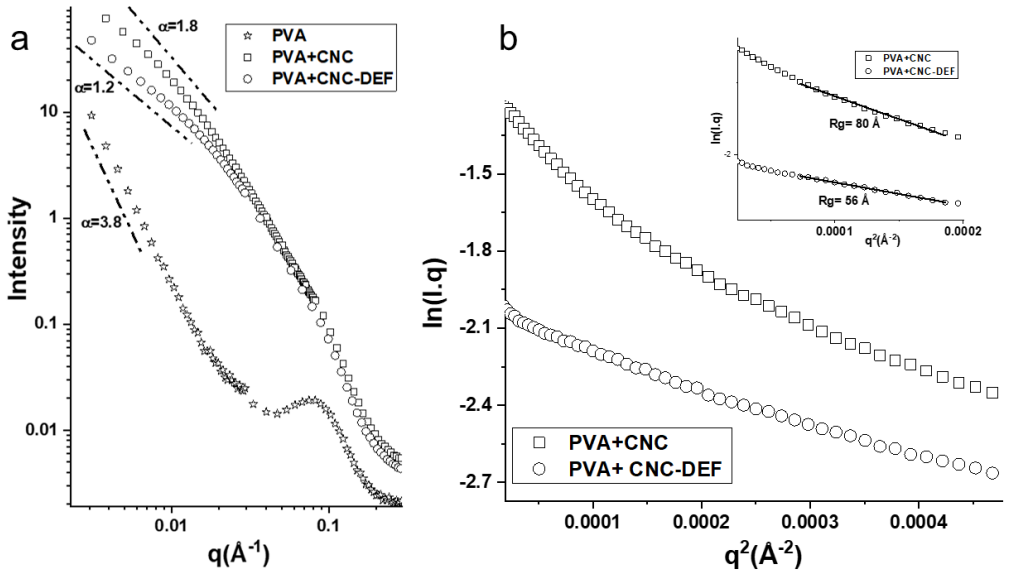


Figure 4. (a) SAXS curves of PVA, PVA+CNC and PVA+CNC-DEF composite films. **(b)** The Guinier analysis of the SAXS curves for PVA + 20 wt% CNC (squares), and PVA+ 20 wt% CNC-DEF (in circle) composite films. The inset in (b) shows the Rg calculation from the Guinier plot.

UV-Blocking Property and Photostability of PVA films

Figure 5a shows the transmittance spectra of neat PVA, PVA+CNC and PVA composite films loaded with varying concentrations of CNC-DEF. PVA alone did not display any appreciable UV protection, as evidenced by the 85-90% transmittance within the UV region. Further, the addition of 20 wt% CNC in PVA did not significantly block the transmittance of UV light. On the other hand, PVA+CNC-DEF composite films display a broad and significant UV absorbance (protection) and high visible light transmittance. This corroborates the study of Sirvio et al.[48] where the addition of 0.5-10 wt% of *p*-aminobenzoic acid-grafted CNCs significantly reduced the UV transmission in PVA films. The UV transmittance spectrum of PVA+CNC-DEF composite films is characterised by two broad peaks at 285 nm and 325 nm which are attributed to diethyl ferulate grafted on CNCs. These values are slightly different from the aqueous suspensions of diethyl ferulate reported previously[19] (300, 326 nm) primarily due to etherification of DEF on CNC and/or solvent or matrix effects.

Figure 5b demonstrates the dependence that the transmittance of UVA (325 nm), UVB (285 nm), and UVC (200 nm) light of the PVA+CNC-DEF films have on the concentration of CNC-DEF added. The optical transmittance of the films generally decreases with increasing CNC-DEF concentration. The addition of 1 wt% CNC-DEF in PVA resulted in an abrupt decrease in transmittance (9-48%) for all wavelengths. In the UVA and UVB regions, further addition of CNC-DEF beyond 1 wt% continually decreases the transmittance until it reaches 0% at a concentration of 20 wt%. Interestingly, the addition of greater than 5wt% CNC-DEF is enough to completely block the transmittance of UVC light.

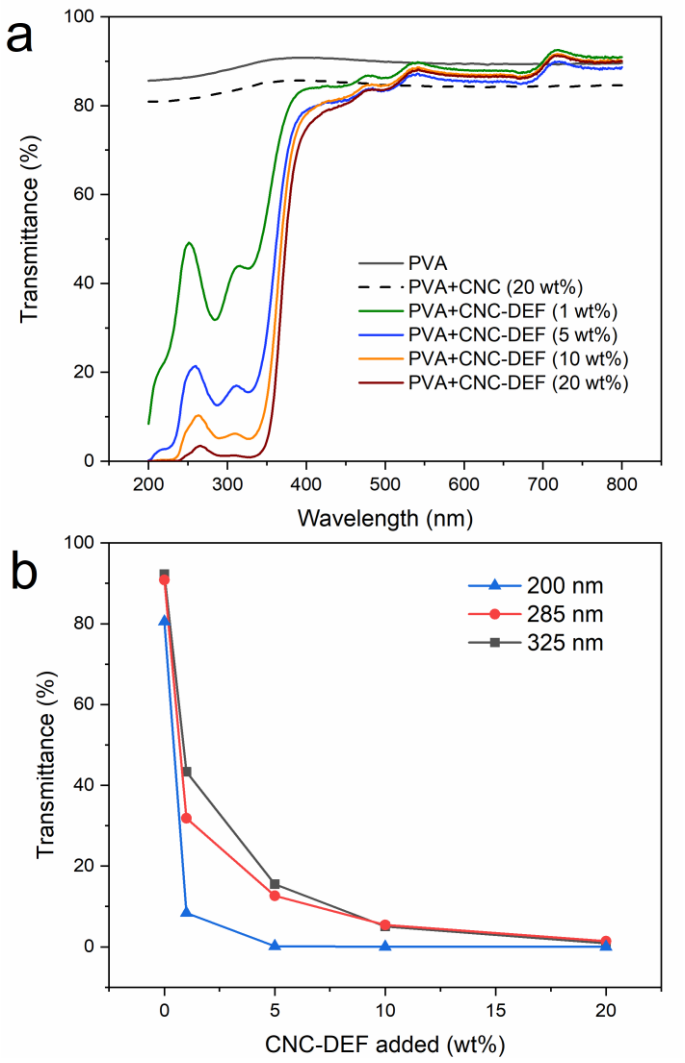


Figure 5. UV-blocking property of PVA+CNC-DEF composite films. **(a)** UV-Vis transmittance spectra of neat PVA, PVA+CNC (20 wt%), and PVA+CNC-DEF (1-20 wt%) composite films. **(b)** Optical transmittance of PVA+CNC-DEF films at different UV wavelengths.

The photostability of the PVA+CNC-DEF (20 wt%) was also investigated by irradiating the films at 365 nm for 2 h. The UV-Vis transmittance spectra of PVA+CNC-DEF films exposed to different UV irradiation times are shown in Figure 6a. The retention of transmittance was recorded as a function of irradiation time and is shown in Figure 6b. The transmittance of the composite film does not appreciably change over time, particularly at 200 nm. Interestingly, even after 2 h of UV irradiation, the PVA+CNC-DEF films remained photostable, with UV transmittance values ranging from 0-1.5%.

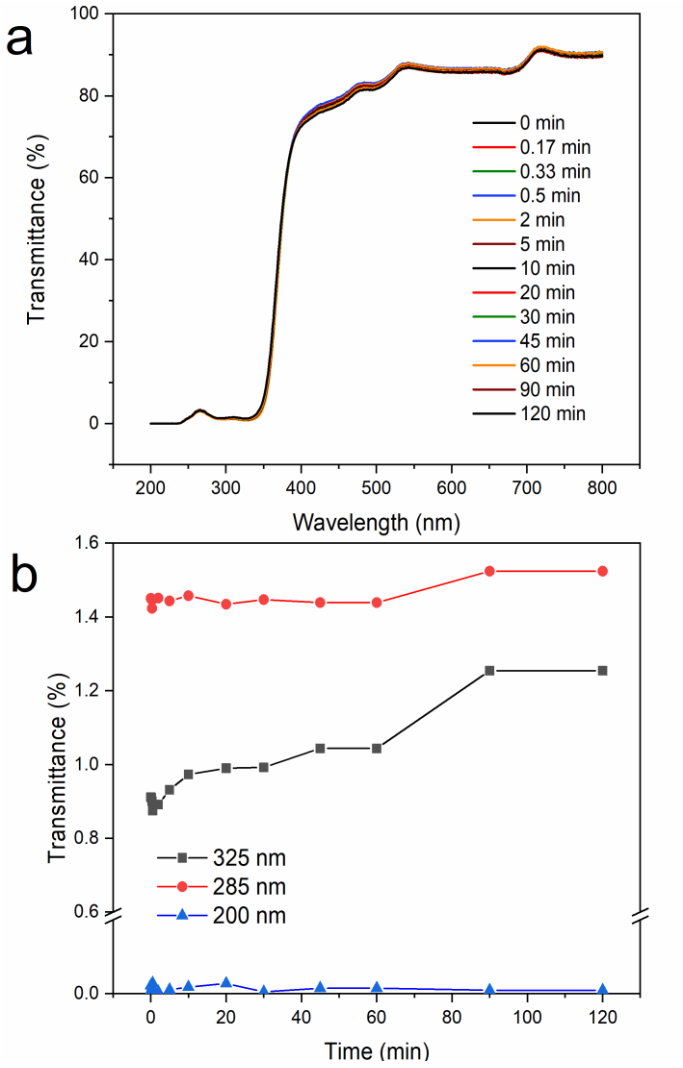


Figure 6. Photostability of PVA+CNC-DEF composite films. **(a)** UV-Vis transmittance spectra of PVA+CNC-DEF (20 wt%) films at different UV-irradiation time. **(b)** Optical transmittance of PVA+CNC-DEF films at different UV wavelengths and UV-irradiation time.

Mechanical Properties and Oxygen Permeability of PVA films

The effect of CNC and CNC-DEF loading on the mechanical properties of PVA composite films was studied. Figure 7a shows the tensile stress-strain curves of neat PVA and PVA loaded with different concentrations of CNC-DEF. The neat PVA displays a typical ductile curve characterised by a plastic deformation region[8, 18, 29]. The addition of different concentrations of pristine CNC or CNC-DEF significantly affected the mechanical properties of the composite film, as shown in Figures 7b-d. In general, the Young's modulus and yield strength of the films increase with increasing filler concentration. The addition of pristine CNC or CNC-DEF promoted a 2.5-147% increase in modulus and 1.4-91% increase in yield strength, relative to neat PVA. Films loaded with pristine CNC exhibit a slightly higher modulus and yield strength compared to those loaded with CNC-DEF. This suggests that grafting DEF

onto CNCs only slightly reduced the reinforcing effect of CNCs on PVA films, likely due to their different polarity. Unlike previous reports[49, 50], the addition of more than 10 wt% CNC or CNC-DEF in PVA did not decrease the tensile strength of the nanocomposite film. This variation can be attributed to differences in film preparation, CNC source, aspect ratio, charge density, and, crystallinity which affect the percolation of CNCs in the polymer matrix[51]. Xu et al.[17] also reported a similar trend in tensile strength when 12 wt% of CNC was added to PVA films.

Increasing the filler concentration decreased the elongation at break of the composite films by 14-68%. In addition, PVA+CNC films have slightly lower elongation at break compared to PVA+CNC-DEF films (except at 10 wt% loading). These results are similar to previous studies on PVA nanocomposite films where the tensile strength improved and elongation decreased after the addition of cellulosic fillers such as microcrystalline cellulose[39], cellulose nanocrystals[52], hemicellulose[17], and cellulose nanofibers[18]. Further, as SEM results reveal (Figure 3), the addition of CNC or CNC-DEF resulted in more densely compact structure which might explain the apparent improvement of the tensile strength of PVA.

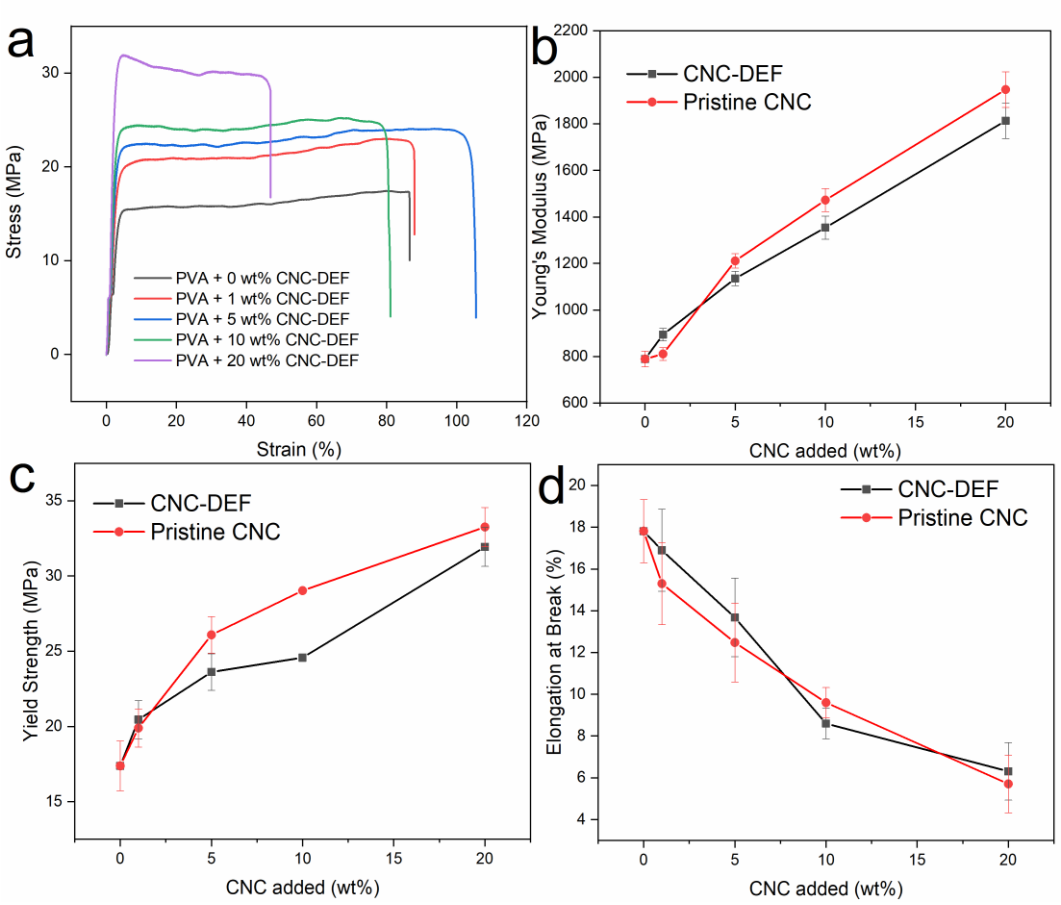


Figure 7. Mechanical properties of neat PVA, PVA+CNC, and PVA+CNC-DEF composite films. **(a)** Tensile stress-strain curves of PVA+CNC-DEF films. Effect of nanofiber

concentration on the **(b)** Young's modulus, **(c)** yield strength, and **(d)** elongation at break of PVA+CNC and PVA+CNC-DEF films.

The oxygen barrier properties of the PVA composite films were also investigated. Figure 8 shows the oxygen permeability of the neat PVA, PVA+CNC, and PVA+CNC-DEF composite films. Neat PVA exhibits a low oxygen permeability of 3.0 $cm^3/m^2.d$ similar to values reported previously[53-55]. The differences observed can be attributed to differences in concentration of PVA, film thickness, and testing conditions such as relative humidity, temperature and pressure. The addition of CNC further increases the oxygen barrier property of PVA, as evidenced by the 33% decrease in oxygen permeability of the PVA+CNC composite film. CNC-DEF addition also decreased the oxygen permeability of PVA film, however, only by 13.33%. These results are similar to the addition of clay (sodium montmorrilonite) in PVA; however, clay can provide better oxygen barrier properties. For example, Grunlan et al. reported that PVA blended with 10 wt% clay has an oxygen permeability of <0.001 cc ·mil/m^2/day at 55% RH[56]. A significant decrease in the oxygen permeability of CNC polymer composites is not likely given its fibrous nature. The effect of CNC addition is not consistent among the reported studies[57]. For example, Fortunati et al [58] described that the addition of 5% CNC decreased the oxygen permeability of polylactic acid (PLA) by 9-48%. However, Espino-Perez et al.[59] reported otherwise that adding up to 15% CNCs generally increased the oxygen permeability of PLA. It was also reported that the addition of 1-2% CNCs decreased the oxygen permeability of polyhydroxy butyrate (PHB) films, but 5% addition caused the opposite effect[60]. Not only does the permeability depend on the presence of the included phase, but the morphology would also change and itself influence permeability, as well as the resultant polarity of the composite. Indeed, SEM results (Figure 3) reveal that CNC or CNC-DEF addition significantly changed the morphology of the PVA film by making the structure more densely compact and less porous, hence, less permeable.

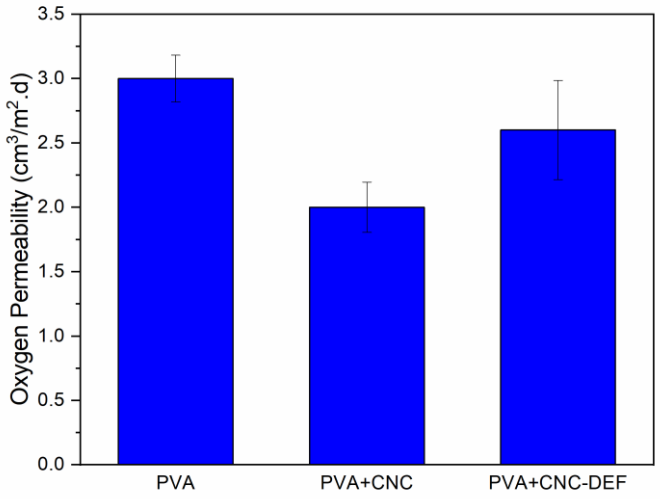


Figure 8. Oxygen permeability of neat PVA, PVA+CNC, PVA+CNC-DEF films at 25 °C, 0% relative humidity, and 1 atm.

DISCUSSION

We report a new class of nanocellulose-based UV-absorbing filler in polyvinyl alcohol films. A few studies have described UV-absorbing nanofillers based on cellulose nanocrystals grafted with cinnamate derivatives. However, the molecules grafted were limited to poly(cinnamoyloxyethyl) methacrylate[28] and cinnamoyl chloride[27]. Here, we decorate cellulose nanocrystals with diethyl ferulate (DEF), a cinnamate diester synthesized from naturally-occurring *p*-hydroxybenzaldehydes using fully-renewable and non-toxic reagents and solvents (Figure S1). DEF was synthesized by a green piperidine/pyridine-free Knoevenagel condensation reaction in ethanol [61]. Further, the synthesis of the DEF-alkyne derivative involves a simple, green, and efficient Williamson etherification reaction (Figure S2). Due to its simplicity, ease, and efficiency, the classical copper-catalyzed azide/alkyne cycloaddition (CuAAC) reaction was used to graft DEF onto cellulose nanocrystals [62, 63]. Indeed, our results show that the click reaction was efficient as evidenced by the 62% conversion of the azide CNC to the corresponding triazole derivative. Theoretically, if the C2 and C3 hydroxyl groups in CNC react, the maximum DS_{surf} achievable is 1.5. This corresponds to 20.67% of DEF covering the CNC surface. Note, however, that a DS_{surf} >1 is unlikely in heterogenous reactions with CNC due to the limited reactivity of the C2 and C3 hydroxyl groups[35]. The incomplete grafting can be attributed to the heterogeneous nature of the reaction and the steric hindrance due to the bulkiness of the phenolic ester moiety[19].

Composite films of PVA+CNC-DEF were prepared *via* a simple solution casting method. Results show that CNC-DEF can be dispersed in the aqueous PVA matrix via ultrasonication prior to casting (Figure S6). The “free” phenolic diester alone, on the other hand, readily aggregates in the PVA solution primarily due to its hydrophobic nature. This shows that grafting the water-insoluble DEF onto water-dispersible CNCs aids in its dispersion in water and PVA due to the hydrophilicity of CNCs based on several types of hydroxyl groups. The colloidal stability of CNC-DEF can also be attributed the negative surface charge arising from the sulfate groups (0.8% S) which were not completely removed after the click reaction. Further, the incorporation of CNC-DEF in the PVA matrix renders the composite film significantly more hydrophobic (Figure 1b). This suggests that CNC-DEF dispersed well within the PVA matrix.

CNCs (and cellulose, in general) have been extensively used as fillers in PVA and other polymeric films[9, 16, 18, 29, 48, 64]. CNCs can form a three-dimensional rigid percolating network within the PVA matrix, owing to the hydroxyl groups present in cellulose[65]. These

hydroxyl groups enable CNCs to self-associate and strongly interact with the PVA molecules *via* hydrogen bonding. In the case of DEF-grafted CNCs, it is likely that the hydrogen bonding interactions between PVA and CNC-DEF are reduced because of the grafted hydrophobic molecule on CNC. SAXS reveals that grafting DEF onto CNC inhibits CNC cluster/aggregation formation and keeps the CNC rods stable (away from each other). This suggests that CNC-DEF have less tendency to form a percolating network within the PVA matrix. This significantly affects the mechanical and oxygen barrier properties of the composite films. Both pristine CNC and CNC-DEF addition significantly improved the modulus and yield strength of the composite films (Figure 7). This is attributed to the good dispersion of the rigid CNCs in the matrix and their strong interaction with PVA *via* hydrogen bonding. However, for CNC-DEF, the hydrogen bonding interactions are reduced in magnitude, leading to slightly lower tensile strength relative to pristine CNC-loaded PVA films. On the contrary, the elongation at break of PVA composite films is significantly diminished after the addition of pristine CNCs or CNC-DEF. This can be attributed to the rigidity of the CNCs which prevents the PVA matrix to further elongate[17, 29, 66]. Interestingly, this diminishing effect in elongation is reduced in the case of CNC-DEF because of the reduced hydrogen bonding interactions.

Further, the addition of pristine CNCs or CNC-DEF decreased the oxygen permeability of PVA films (Figure 8). CNCs act as nanofillers in the PVA matrix ─ they enhance the barrier properties of the film by filling up the pores and slightly increasing the film tortuosity, thereby slowing or inhibiting the permeation process of oxygen molecules[29]. Grafting DEF onto CNCs, however, slightly reduced the oxygen barrier property of the PVA composite film relative to pristine CNC-loaded PVA films. Similarly, this can be a consequence of reduced hydrogen bonding interactions of CNC-DEF with PVA. Relative to pristine CNCs, CNC-DEF does not tightly fill up the voids within the PVA matrix resulting in some free volume where oxygen can slowly permeate. Nevertheless, the oxygen barrier properties of PVA still improved after CNC-DEF addition and the resulting composite film remains excellent for packaging applications.

The addition of CNC-DEF in the PVA matrix transformed the originally UV-inert film into strongly UV-blocking material (Figure 5). The UV-shielding property of the composite film is solely attributed to the DEF grafted on CNCs, as the addition of pristine CNCs did not provide any significant UV protection. The UV transmittance spectrum of PVA+CNC-DEF composite films is characterised by two broad peaks at 285 nm and 325 nm which cover both UVA and UVB regions. This is particularly important as there is already a considerable number of UVB filters, but a scarcity of effective UVA filters[20]. In this work, we have demonstrated that at 20 wt% CNC-DEF addition, the composite films can block the transmittance of light in the UVA, UVB, and UVC regions without appreciable changes in the high visible transparency. Further, steady-state irradiation experiments show the excellent photostability of the

composite films over the whole UV range. This is primarily attributed to the high photostability of DEF which can undergo an efficient *trans-cis* and *cis-trans* photoisomerization, resulting in a photo-equilibrium between the isomers[67-69]. These results show that the reinforcement of CNC-DEF in PVA films does not impede its excellent photostability observed in our previous study[19].

This study shows that CNCs grafted with diethyl ferulate are excellent UV-absorbing and reinforcement nanofillers in polyvinyl alcohol films (Figure 9). Reinforcement of CNC-DEF in PVA produces highly-transparent films with excellent photostability and UV-absorbing properties (0% UV transmittance). Furthermore, the addition of CNC-DEF significantly improves the tensile properties of PVA films by almost 90-150% relative to neat PVA. The oxygen permeability of the composite films is also reduced after CNC-DEF addition. Overall, this study reports a new generation of multifunctional nanofillers for the development of sustainable materials for industrial and food packaging applications.

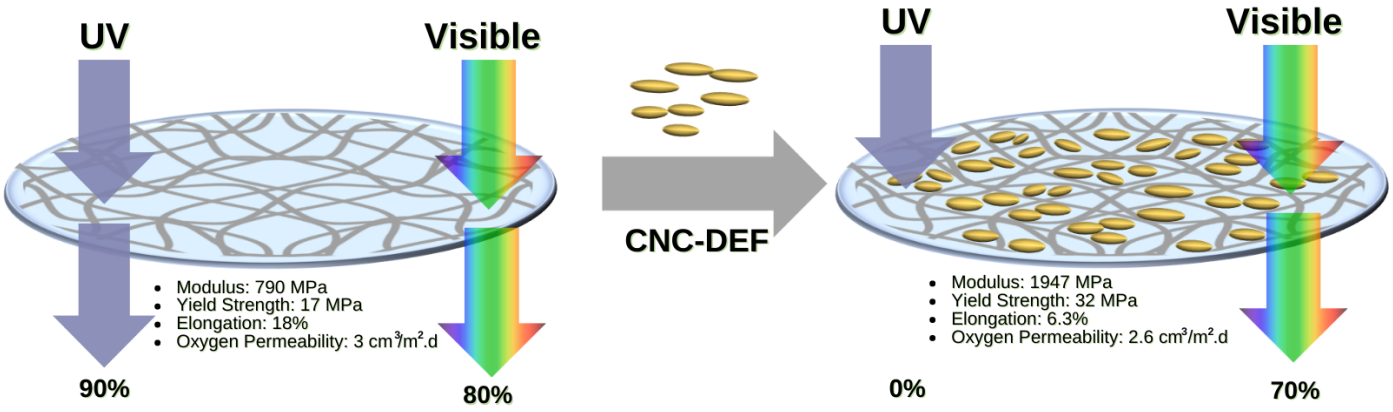


Figure 9. Schematic representation of the UV-blocking and reinforcing effect of CNC-DEF addition (20 wt%) in PVA. The oxygen barrier properties of the composite film are also depicted.

CONCLUSION

We report a novel multifunctional nanofiller as reinforcement in polyvinyl alcohol films based on phenolic ester-grafted cellulose nanocrystals. Click-type copper-catalyzed azide/alkyne cycloaddition (CuAAC) reactions were used to decorate cellulose nanocrystals with diethyl ferulate (DEF) ─ a cinnamate diester synthesized from naturally-occurring *p*-hydroxybenzaldehydes using fully-renewable and non-toxic reagents and solvents. Grafting the water-insoluble DEF onto water-dispersible CNCs aids its dispersion in water and PVA. CNCs decorated with DEF (CNC-DEF) could be well dispersed in the aqueous PVA matrix via

ultrasonication, prior to casting. Similar to pristine CNCs, CNC-DEF can form a three-dimensional rigid percolating network within the PVA matrix, albeit with reduced secondary hydrogen bonding interactions due to grafting of the DEF molecule. SAXS reveals that CNC-DEF particles tend to repel each other and generate less interactions with the PVA matrix. Mechanical tests show that the addition of 20 wt% CNC-DEF in PVA increases the tensile strength and modulus by 91% and 150%, respectively, relative to neat PVA. In addition, the oxygen permeability of PVA films reduced after CNC-DEF addition. Interestingly, the addition of CNC-DEF in the PVA matrix transformed the originally UV-inert film into a strongly UV-blocking material. CNC-DEF-loaded PVA composite films reveal excellent photostability and strong and broad UV-blocking properties. PVA+CNC-DEF (20 wt%) composite films exhibit complete UV protection (0% transmittance) and high transparency in the visible region (70-90% transmittance). This study ultimately demonstrates the synergistic UV-blocking effect of diethyl ferulate and the reinforcing effect of cellulose nanocrystals in PVA composite films. These nature-inspired nanofibrillar additives can be integrated into polymeric films to engineer cost-effective, lightweight, and multifunctional materials for scalable industrial and packaging applications.

ACKNOWLEDGEMENT

Funding from the Australian Research Council-Industry Transformation Research Hub; Processing Advanced Lignocellulosics (PALS) [grant number IH130100016] is gratefully acknowledged. The authors acknowledge the use of the instruments and scientific and technical assistance of X. Fang at the Monash Centre for Electron Microscopy, a Node of Microscopy Australia. A part of this research was undertaken on the SAXS/WAXS beamline at the Australian Synchrotron, part of ANSTO. D. Mendoza is grateful to URD ABI for hosting him for ca. 4 months. The authors also thank Grand Reims and Région Grand Est for their financial support.

REFERENCES

1. Pastoriza-Santos, I.; Kinnear, C.; Pérez-Juste, J.; Mulvaney, P.; Liz-Marzán, L. M., Plasmonic polymer nanocomposites. *Nat. Rev. Mater.* 2018, *3* (10), 375-391. DOI: https://doi.org/10.1038/s41578-018-0050-7.

2. Harito, C.; Bavykin, D. V.; Yuliarto, B.; Dipojono, H. K.; Walsh, F. C., Polymer nanocomposites having a high filler content: synthesis, structures, properties, and applications. *Nanoscale* 2019, *11* (11), 4653-4682. DOI: https://doi.org/10.1039/C9NR00117D.

3. Fu, S.; Sun, Z.; Huang, P.; Li, Y.; Hu, N., Some basic aspects of polymer nanocomposites: A critical review. *Nano Mater. Sci.* 2019, *1* (1), 2-30. DOI: https://doi.org/10.1016/j.nanoms.2019.02.006.

4. Crosby, A. J.; Lee, J. Y., Polymer Nanocomposites: The "Nano" Effect on Mechanical Properties. *Polym. Rev.* 2007, *47* (2), 217-229. DOI: https://doi.org/10.1080/15583720701271278.
5. Aslam, M.; Kalyar, M. A.; Raza, Z. A., Polyvinyl alcohol: A review of research status and use of polyvinyl alcohol based nanocomposites. *Polym. Eng. Sci.* 2018, *58* (12), 2119-2132. DOI: https://doi.org/10.1002/pen.24855.
6. Iqbal, T.; Irfan, M.; Ramay, S. M.; Mahmood, A.; Saleem, M.; Siddiqi, S. A., ZnO–PVA Polymer Matrix with Transition Metals Oxide Nano-fillers for High Dielectric Mediums. *J. Polym. Environ.* 2020, *28* (9), 2422-2432. DOI: https://doi.org/10.1007/s10924-020-01768-x.
7. Jayakumar, A.; Heera, K. V.; T.S, S.; Joseph, M.; Mathew, S.; Praveen, G.; Nair, I. C.; Radhakrishnan, E. K., Starch-PVA composite films with zinc-oxide nanoparticles and phytochemicals as intelligent pH sensing wraps for food packaging application. *Int. J. Biol. Macromol.* 2019, *136*, 395-403. DOI: https://doi.org/10.1016/j.ijbiomac.2019.06.018.
8. Panova, T. V.; Efimova, A. A.; Berkovich, A. K.; Efimov, A. V., Plasticity control of poly(vinyl alcohol)–graphene oxide nanocomposites. *RSC Adv.* 2020, *10* (40), 24027-24036. DOI: https://doi.org/10.1039/D0RA04150E.
9. Aloui, H.; Khwaldia, K.; Hamdi, M.; Fortunati, E.; Kenny, J. M.; Buonocore, G. G.; Lavorgna, M., Synergistic Effect of Halloysite and Cellulose Nanocrystals on the Functional Properties of PVA Based Nanocomposites. *ACS Sustainable Chem. Eng.* 2016, *4* (3), 794-800. DOI: https://doi.org/10.1021/acssuschemeng.5b00806.
10. Spagnol, C.; Fragal, E. H.; Witt, M. A.; Follmann, H. D. M.; Silva, R.; Rubira, A. F., Mechanically improved polyvinyl alcohol-composite films using modified cellulose nanowhiskers as nano-reinforcement. *Carbohydr. Polym.* 2018, *191*, 25-34. DOI: https://doi.org/10.1016/j.carbpol.2018.03.001.
11. Virtanen, S.; Vartianen, J.; Setälä, H.; Tammelin, T.; Vuoti, S., Modified nanofibrillated cellulose–polyvinyl alcohol films with improved mechanical performance. *RSC Adv.* 2014, *4* (22), 11343-11350. DOI: https://doi.org/10.1039/C3RA46287K.
12. Klemm, D.; Schumann, D.; Kramer, F.; Heßler, N.; Koth, D.; Sultanova, B., Nanocellulose Materials – Different Cellulose, Different Functionality. *Macromol. Symp.* 2009, *280* (1), 60-71. DOI: https://doi.org/10.1002/masy.200950608.
13. Dufresne, A., Nanocellulose: a new ageless bionanomaterial. *Mater. Today* 2013, *16* (6), 220-227. DOI: https://doi.org/10.1016/j.mattod.2013.06.004.
14. Mendoza, D. J.; Browne, C.; Raghuwanshi, V. S.; Simon, G. P.; Garnier, G., One-shot TEMPO-periodate oxidation of native cellulose. *Carbohydr. Polym.* 2019, *226*, 115292. DOI: https://doi.org/10.1016/j.carbpol.2019.115292.
15. Mendoza, D. J.; Hossain, L.; Browne, C.; Raghuwanshi, V. S.; Simon, G. P.; Garnier, G., Controlling the transparency and rheology of nanocellulose gels with the extent of carboxylation. *Carbohydr. Polym.* 2020, *245*, 116566. DOI: https://doi.org/10.1016/j.carbpol.2020.116566.

16. Fortunati, E.; Puglia, D.; Monti, M.; Santulli, C.; Maniruzzaman, M.; Kenny, J. M., Cellulose nanocrystals extracted from okra fibers in PVA nanocomposites. *J. Appl. Polym. Sci.* 2013, *128* (5), 3220-3230. DOI: https://doi.org/10.1002/app.38524.
17. Xu, S.; Jiang, M.; Lu, Q.; Gao, S.; Feng, J.; Wang, X.; He, X.; Chen, K.; Li, Y.; Ouyang, P., Properties of Polyvinyl Alcohol Films Composited With Hemicellulose and Nanocellulose Extracted From Artemisia selengensis Straw. *Front. Bioeng. Biotechnol.* 2020, *8*, 980. DOI: https://doi.org/10.3389/fbioe.2020.00980.
18. Liu, D.; Sun, X.; Tian, H.; Maiti, S.; Ma, Z., Effects of cellulose nanofibrils on the structure and properties on PVA nanocomposites. *Cellulose* 2013, *20* (6), 2981-2989. DOI: https://doi.org/10.1007/s10570-013-0073-6.
19. Mendoza, D. J.; Mouterde, L. M. M.; Browne, C.; Raghuwanshi, V. S.; Simon, G. P.; Garnier, G.; Allais, F., Grafting Nature-Inspired and Bio-Based Phenolic Esters onto Cellulose Nanocrystals Gives Biomaterials with Photostable Anti-UV Properties. *ChemSusChem* 2020, *13* (24), 6552-6561. DOI: https://doi.org/10.1002/cssc.202002017.
20. Horbury, M. D.; Holt, E. L.; Mouterde, L. M. M.; Balaguer, P.; Cebrian, J.; Blasco, L.; Allais, F.; Stavros, V. G., Towards symmetry driven and nature inspired UV filter design. *Nat. Commun.* 2019, *10* (1), 4748. DOI: https://doi.org/10.1038/s41467-019-12719-z.
21. Flourat, A. L.; Combes, J.; Bailly-Maitre-Grand, C.; Magnien, K.; Haudrechy, A.; Renault, J.-H.; Allais, F., Accessing p-Hydroxycinnamic Acids: Chemical Synthesis, Biomass Recovery, or Engineered Microbial Production? *ChemSusChem* 2021, *14* (1), 118-129. DOI: https://doi.org/10.1002/cssc.202002141.
22. Peyrot, C.; Mention, M. M.; Brunissen, F.; Allais, F., Sinapic Acid Esters: Octinoxate Substitutes Combining Suitable UV Protection and Antioxidant Activity. *Antioxidants* 2020, *9* (9), 782. DOI: https://doi.org/10.3390/antiox9090782.
23. Sadeghifar, H.; Venditti, R.; Jur, J.; Gorga, R. E.; Pawlak, J. J., Cellulose-Lignin Biodegradable and Flexible UV Protection Film. *ACS Sustainable Chem. Eng.* 2017, *5* (1), 625-631. DOI: https://doi.org/10.1021/acssuschemeng.6b02003.
24. Kaler, V.; Pandel, U.; Duchaniya, R. K., Development of TiO_2/PVA nanocomposites for application in solar cells. *Mater. Today: Proc.* 2018, *5* (2, Part 1), 6279-6287. DOI: https://doi.org/10.1016/j.matpr.2017.12.237.
25. Schneider, S. L.; Lim, H. W., A review of inorganic UV filters zinc oxide and titanium dioxide. *Photodermatol., Photoimmunol. Photomed.* 2019, *35* (6), 442-446. DOI: https://doi.org/10.1111/phpp.12439.
26. Zhao, H.; Li, R. K. Y., A study on the photo-degradation of zinc oxide (ZnO) filled polypropylene nanocomposites. *Polymer* 2006, *47* (9), 3207-3217. DOI: https://doi.org/10.1016/j.polymer.2006.02.089.
27. Zhang, Z.; Zhang, B.; Grishkewich, N.; Berry, R.; Tam, K. C., Cinnamate-Functionalized Cellulose Nanocrystals as UV-Shielding Nanofillers in Sunscreen and Transparent Polymer Films. *Adv. Sustainable Syst.* 2019, *3* (4), 1800156. DOI: https://doi.org/10.1002/adsu.201800156.

28. Zhang, Z.; Sèbe, G.; Wang, X.; Tam, K. C., UV-Absorbing Cellulose Nanocrystals as Functional Reinforcing Fillers in Poly(vinyl chloride) Films. *ACS Appl. Nano Mater.* 2018, *1* (2), 632-641. DOI: https://doi.org/10.1021/acsanm.7b00126.
29. Yang, W.; Qi, G.; Kenny, J. M.; Puglia, D.; Ma, P., Effect of Cellulose Nanocrystals and Lignin Nanoparticles on Mechanical, Antioxidant and Water Vapour Barrier Properties of Glutaraldehyde Crosslinked PVA Films. *Polymers* 2020, *12* (6), 1364. DOI: https://doi.org/10.3390/polym12061364.
30. Guo, Y.; Tian, D.; Shen, F.; Yang, G.; Long, L.; He, J.; Song, C.; Zhang, J.; Zhu, Y.; Huang, C.; Deng, S., Transparent Cellulose/Technical Lignin Composite Films for Advanced Packaging. *Polymers* 2019, *11* (9), 1455. DOI: https://doi.org/10.3390/polym11091455.
31. Zhang, Z.; Zhang, B.; Grishkewich, N.; Berry, R.; Tam, K. C., Cinnamate-Functionalized Cellulose Nanocrystals as UV-Shielding Nanofillers in Sunscreen and Transparent Polymer Films. *Adv. Sustainable Syst.* 2019, *3* (4). DOI: 10.1002/adsu.201800156.
32. Mouterde, L. M. M.; Allais, F., Microwave-Assisted Knoevenagel-Doebner Reaction: An Efficient Method for Naturally Occurring Phenolic Acids Synthesis. *Front. Chem.* 2018, *6*, 426. DOI: https://doi.org/10.3389/fchem.2018.00426.
33. Irfan, M.; Aneja, B.; Yadava, U.; Khan, S. I.; Manzoor, N.; Daniliuc, C. G.; Abid, M., Synthesis, QSAR and anticandidal evaluation of 1,2,3-triazoles derived from naturally bioactive scaffolds. *Eur. J. Med. Chem.* 2015, *93*, 246-254. DOI: https://doi.org/10.1016/j.ejmech.2015.02.007.
34. Missoum, K.; Belgacem, M. N.; Barnes, J.-P.; Brochier-Salon, M.-C.; Bras, J., Nanofibrillated cellulose surface grafting in ionic liquid. *Soft Matter* 2012, *8* (32). DOI: https://doi.org/10.1039/c2sm25691f.
35. Eyley, S.; Thielemans, W., Surface modification of cellulose nanocrystals. *Nanoscale* 2014, *6* (14), 7764-79. DOI: 10.1039/c4nr01756k.
36. Feese, E.; Sadeghifar, H.; Gracz, H. S.; Argyropoulos, D. S.; Ghiladi, R. A., Photobactericidal porphyrin-cellulose nanocrystals: synthesis, characterization, and antimicrobial properties. *Biomacromolecules* 2011, *12* (10), 3528-39. DOI: 10.1021/bm200718s.
37. Sadeghifar, H.; Filpponen, I.; Clarke, S. P.; Brougham, D. F.; Argyropoulos, D. S., Production of cellulose nanocrystals using hydrobromic acid and click reactions on their surface. *J. Mater. Sci.* 2011, *46* (22), 7344-7355. DOI: https://doi.org/10.1007/s10853-011-5696-0.
38. Eyley, S.; Shariki, S.; Dale, S. E.; Bending, S.; Marken, F.; Thielemans, W., Ferrocene-decorated nanocrystalline cellulose with charge carrier mobility. *Langmuir* 2012, *28* (16), 6514-9. DOI: 10.1021/la3001224.
39. Sun, X.; Lu, C.; Liu, Y.; Zhang, W.; Zhang, X., Melt-processed poly(vinyl alcohol) composites filled with microcrystalline cellulose from waste cotton fabrics. *Carbohydr. Polym.* 2014, *101*, 642-649. DOI: https://doi.org/10.1016/j.carbpol.2013.09.088.
40. Chhatri, A.; Bajpai, J.; Bajpai, A. K.; Sandhu, S. S.; Jain, N.; Biswas, J., Cryogenic fabrication of savlon loaded macroporous blends of alginate and polyvinyl alcohol

(PVA). Swelling, deswelling and antibacterial behaviors. *Carbohydr. Polym.* 2011, *83* (2), 876-882. DOI: https://doi.org/10.1016/j.carbpol.2010.08.077.
41. Lambert, J. B.; Gronert, S.; Shurvell, H. F.; Lightner, D.; Cooks, R. G., *Organic Structural Spectroscopy*. 2 ed.; Pearson: 2013.
42. Glatter, O.; Kratky, O.; Kratky, H. C., *Small Angle X-ray Scattering*. Academic Press: 1982.
43. Raghuwanshi, V. S.; Garusinghe, U. M.; Raj, P.; Kirby, N.; Hoell, A.; Batchelor, W.; Garnier, G., Cationic polyacrylamide induced nanoparticles assembly in a cellulose nanofiber network. *J. Colloid Interface Sci.* 2018, *529*, 180-186. DOI: https://doi.org/10.1016/j.jcis.2018.06.009.
44. Raghuwanshi, V. S.; Harizanova, R.; Tatchev, D.; Hoell, A.; Rüssel, C., Structural analysis of Fe–Mn–O nanoparticles in glass ceramics by small angle scattering. *J. Solid State Chem.* 2015, *222*, 103-110. DOI: https://doi.org/10.1016/j.jssc.2014.11.009.
45. Otsuka, E.; Sugiyama, M.; Suzuki, A., Network Microstructure of PVA Cast Gels Observed by SAXS Measurements. *J. Phys.: Conf. Ser.* 2010, *247*, 012043. DOI: https://doi.org/10.1088/1742-6596/247/1/012043.
46. Andrade, G. I.; Barbosa-Stancioli, E. F.; Mansur, A. A. P.; Vasconcelos, W. L.; Mansur, H. S., Small-angle X-ray scattering and FTIR characterization of nanostructured poly (vinyl alcohol)/silicate hybrids for immunoassay applications. *J. Mater. Sci.* 2008, *43* (2), 450-463. DOI: https://doi.org/10.1007/s10853-007-1953-7.
47. Rodrigues, A. P. H.; Pereira, I. M.; de Souza, S. D.; Gil, C. S. B.; Machado, G.; Carvalho, S. M.; Pereira, F. V.; Paiva, P. R. P.; de Oliveira, L. C. A.; de O. Patricio, P. S., Control of properties of nanocomposites bio-based collagen and cellulose nanocrystals. *Cellulose* 2017, *24* (4), 1731-1744. DOI: https://doi.org/10.1007/s10570-017-1218-9.
48. Sirviö, J. A.; Visanko, M.; Heiskanen, J. P.; Liimatainen, H., UV-absorbing cellulose nanocrystals as functional reinforcing fillers in polymer nanocomposite films. *J. Mater. Chem. A* 2016, *4* (17), 6368-6375. DOI: https://doi.org/10.1039/c6ta00900j.
49. Rahman, M. M.; Afrin, S.; Haque, P., Characterization of crystalline cellulose of jute reinforced poly (vinyl alcohol) (PVA) biocomposite film for potential biomedical applications. *Prog. Biomater.* 2014, *3* (1), 23. DOI: 10.1007/s40204-014-0023-x.
50. Lee, S.-Y.; Mohan, D. J.; Kang, I.-A.; Doh, G.-H.; Lee, S.; Han, S. O., Nanocellulose reinforced PVA composite films: Effects of acid treatment and filler loading. *Fibers. Polym.* 2009, *10* (1), 77-82. DOI: 10.1007/s12221-009-0077-x.
51. Silvério, H. A.; Flauzino Neto, W. P.; Dantas, N. O.; Pasquini, D., Extraction and characterization of cellulose nanocrystals from corncob for application as reinforcing agent in nanocomposites. *Ind. Crops Prod.* 2013, *44*, 427-436. DOI: https://doi.org/10.1016/j.indcrop.2012.10.014.
52. Fortunati, E.; Puglia, D.; Luzi, F.; Santulli, C.; Kenny, J. M.; Torre, L., Binary PVA bio-nanocomposites containing cellulose nanocrystals extracted from different natural sources: Part I. *Carbohydr. Polym.* 2013, *97* (2), 825-836. DOI: https://doi.org/10.1016/j.carbpol.2013.03.075.

53. Massey, L. K., Chapter 49 - Polyvinyl Alcohol (PVOH). In *Permeability Properties of Plastics and Elastomers (Second Edition)*, Massey, L. K., Ed. William Andrew Publishing: Norwich, NY, 2003; pp 297-298.
54. Ding, J.; Zhang, R.; Ahmed, S.; Liu, Y.; Qin, W., Effect of Sonication Duration in the Performance of Polyvinyl Alcohol/Chitosan Bilayer Films and Their Effect on Strawberry Preservation. *Molecules* 2019, *24* (7), 1408. DOI: https://doi.org/10.3390/molecules24071408.
55. Liu, Y.; Wang, S.; Lan, W.; Qin, W., Fabrication and Testing of PVA/Chitosan Bilayer Films for Strawberry Packaging. *Coatings* 2017, *7* (8), 109. DOI: https://doi.org/10.3390/coatings7080109.
56. Grunlan, J. C.; Grigorian, A.; Hamilton, C. B.; Mehrabi, A. R., Effect of clay concentration on the oxygen permeability and optical properties of a modified poly(vinyl alcohol). *J. Appl. Polym. Sci.* 2004, *93* (3), 1102-1109. DOI: https://doi.org/10.1002/app.20564.
57. Wang, J.; Gardner, D. J.; Stark, N. M.; Bousfield, D. W.; Tajvidi, M.; Cai, Z., Moisture and Oxygen Barrier Properties of Cellulose Nanomaterial-Based Films. *ACS Sustainable Chem. Eng.* 2018, *6* (1), 49-70. DOI: https://doi.org/10.1021/acssuschemeng.7b03523.
58. Fortunati, E.; Peltzer, M.; Armentano, I.; Torre, L.; Jiménez, A.; Kenny, J. M., Effects of modified cellulose nanocrystals on the barrier and migration properties of PLA nano-biocomposites. *Carbohydr. Polym.* 2012, *90* (2), 948-956. DOI: https://doi.org/10.1016/j.carbpol.2012.06.025.
59. Espino-Pérez, E.; Bras, J.; Ducruet, V.; Guinault, A.; Dufresne, A.; Domenek, S., Influence of chemical surface modification of cellulose nanowhiskers on thermal, mechanical, and barrier properties of poly(lactide) based bionanocomposites. *Eur. Polym. J.* 2013, *49* (10), 3144-3154. DOI: https://doi.org/10.1016/j.eurpolymj.2013.07.017.
60. Dhar, P.; Bhardwaj, U.; Kumar, A.; Katiyar, V., Poly (3-hydroxybutyrate)/cellulose nanocrystal films for food packaging applications: Barrier and migration studies. *Polym. Eng. Sci.* 2015, *55* (10), 2388-2395. DOI: https://doi.org/10.1002/pen.24127.
61. Peyrot, C.; Peru, A. A. M.; Mouterde, L. M. M.; Allais, F., Proline-Mediated Knoevenagel–Doebner Condensation in Ethanol: A Sustainable Access to p-Hydroxycinnamic Acids. *ACS Sustainable Chem. Eng.* 2019, *7* (10), 9422-9427. DOI: https://doi.org/10.1021/acssuschemeng.9b00624.
62. Neumann, S.; Biewend, M.; Rana, S.; Binder, W. H., The CuAAC: Principles, Homogeneous and Heterogeneous Catalysts, and Novel Developments and Applications. *Macromol. Rapid Commun.* 2020, *41* (1), e1900359. DOI: https://doi.org/10.1002/marc.201900359.
63. Filpponen, I., Click Chemistry in Cellulose Functionalization. In *Handbook of Green Materials*, World Scientific: 2013; Vol. 5, pp 19-36.
64. Peresin, M. S.; Vesterinen, A.-H.; Habibi, Y.; Johansson, L.-S.; Pawlak, J. J.; Nevzorov, A. A.; Rojas, O. J., Crosslinked PVA nanofibers reinforced with cellulose

nanocrystals: Water interactions and thermomechanical properties. *J. Appl. Polym. Sci.* 2014, *131* (11), 40334. DOI: https://doi.org/10.1002/app.40334.
65. Khan, A.; Huq, T.; Khan, R. A.; Riedl, B.; Lacroix, M., Nanocellulose-based composites and bioactive agents for food packaging. *Crit. Rev. Food Sci. Nutr.* 2014, *54* (2), 163-74. DOI: 10.1080/10408398.2011.578765.
66. Rescignano, N.; Fortunati, E.; Montesano, S.; Emiliani, C.; Kenny, J. M.; Martino, S.; Armentano, I., PVA bio-nanocomposites: A new take-off using cellulose nanocrystals and PLGA nanoparticles. *Carbohydr. Polym.* 2014, *99*, 47-58. DOI: https://doi.org/10.1016/j.carbpol.2013.08.061.
67. Kuramochi, H.; Takeuchi, S.; Tahara, T., Ultrafast Structural Evolution of Photoactive Yellow Protein Chromophore Revealed by Ultraviolet Resonance Femtosecond Stimulated Raman Spectroscopy. *J. Phys. Chem. Lett.* 2012, *3* (15), 2025-2029. DOI: https://doi.org/10.1021/jz300542f.
68. Espagne, A.; Changenet-Barret, P.; Plaza, P.; Martin, M. M., Solvent Effect on the Excited-State Dynamics of Analogues of the Photoactive Yellow Protein Chromophore. *J. Phys. Chem. A* 2006, *110* (10), 3393-3404. DOI: https://doi.org/10.1021/jp0563843.
69. Horbury, M. D.; Baker, L. A.; Rodrigues, N. D. N.; Quan, W.-D.; Stavros, V. G., Photoisomerization of ethyl ferulate: A solution phase transient absorption study. *Chem. Phys. Lett.* 2017, *673*, 62-67. DOI: https://doi.org/10.1016/j.cplett.2017.02.004.

CONTRIBUTIONS

F. Allais, L. M. M. Mouterde, and G. Garnier conceived the first phase of the project. G. P. Simon, and G. Garnier supervised this project. F. Allais, L. M. M. Mouterde, and D. J. Mendoza designed the synthesis of diethyl ferulate and the click reaction. D. J. Mendoza performed the experiments and characterization of the films. D. J. Mendoza and C. Browne performed the tensile tests and optical profilometry. V. S. Raghuwanshi, D. J. Mendoza, and G. Garnier performed the SAXS experiments. D. J. Mendoza wrote the first draft of the manuscript. All the authors discussed the results and commented on the manuscript.

CONFLICT OF INTEREST

The authors declare no conflict of interest.

ORCID

David Joram Mendoza 0000-0002-7959-0837

Christine Browne 0000-0002-1867-8413

Vikram Singh Raghuwanshi 0000-0001-9524-1314

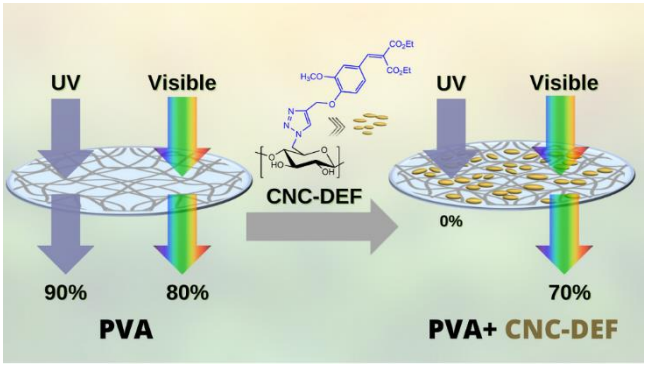
Louis M.M. Mouterde 0000-0002-4096-1629

Florent Allais 0000-0003-4132-6210

George P. Simon 0000-0001-8832-1164

Gil Garnier 0000-0003-3512-0056

TOC



This study reports the incorporation of nature-inspired phenolic ester-grafted CNCs in PVA to engineer performant UV-blocking polymer films.